Landsat Radiometric Processing Enhancements and Updates

B. Markham[1], J. Barsi[1,2], R. Morfitt[3], E. Micijevic, Md[4], O. Haque[4], M. Montanaro[5], A. Gerace[5], D. Helder[6], J. Czapla-Myers[7], and S. Biggar[7],

[1]Biospheric Sciences, NASA GSFC, [2]SSAI, [3]USGS, [4]SGT/EROS, [5]RIT, [6]SDSU, [7]U. of Arizona

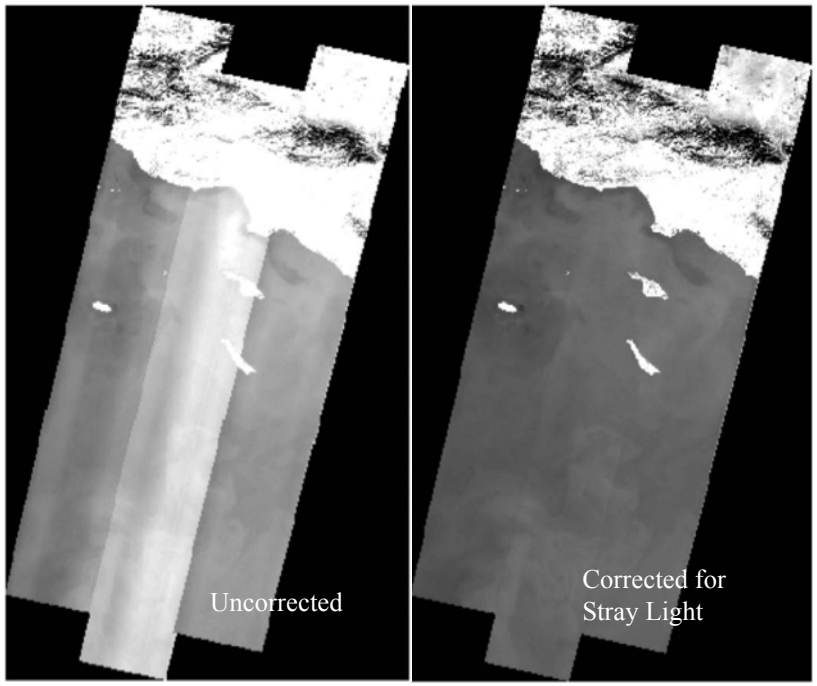

Figure 1

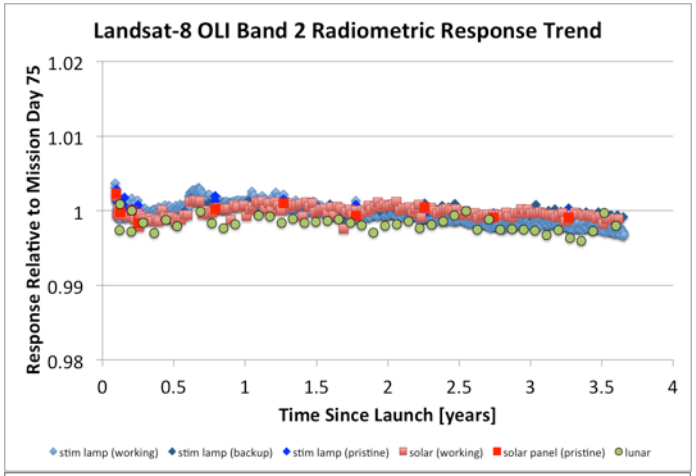

Figure 2

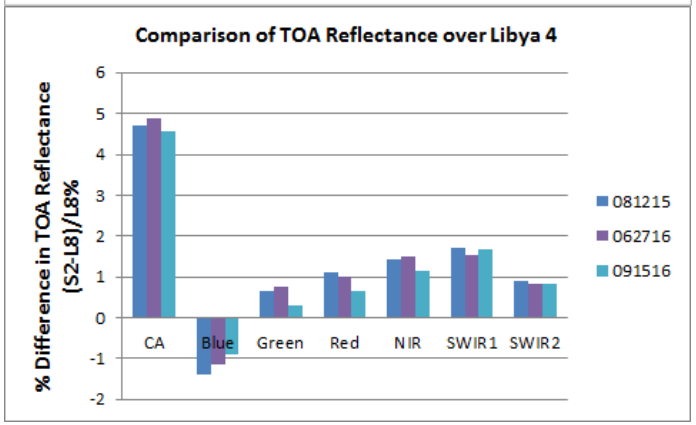

Figure 3

Landsat operational processing will now include correction for Landsat-8 TIRS stray light and provide consistent Landsat-4 TM to Landsat-7 ETM+ radiometric calibration tied to the Landsat-8 OLI reflectance calibration. Landsat-8 OLI is radiometrically stable and consistent with Sentinel-2 MSI.

Name: Brian L. Markham, Biospheric Sciences, NASA GSFC
E-mail: Brian.L.Markham@nasa.gov,
Phone: 301-614-6608

References:

2016 Montanaro, M., Gerace, A. (2016) Performance of the proposed stray light correction algorithm for the thermal infrared sensor (TIRS) onboard Landsat 8. *Proc. SPIE 9972, Earth Observing Systems XXI*, 99720F1-7; doi:10.1117/12.2238554.

2016 Micijevic, E., Haque, Md O., Mishra, N. (2016) Radiometric Calibration Updates to the Landsat Collection. *Proc. SPIE 9972, Earth Observing Systems XXI*, 99720D1-12; doi:10.1117/12.2239426.

2015 Markham, B., Barsi, J., Kaita, E., Ong, L., Morfitt, R., Haque, Md O. (2015). Radiometric Calibration and Stability of the Landsat-8 Operational Land Imager(OLI). Proc. SPIE 9607, Earth Observing Systems XX, 96070N-1-7; doi:10.1117/12.2188412.

2015 Montanaro, M., Gerace, A., Rohrbach, S. (2015) Toward an operational stray light correction for the Landsat 8 Thermal Infrared Sensor. *Applied Optics*, 54, 3963-3978.

2015 Czapla-Myers, J., McCorkel, J., Anderson, N., Biggar, S., Helder, D., Aaron, D., Leigh, L., Mishra, N. (2015) The Ground-Based Absolute Radiometric Calibration of Landsat 8 OLI. *Remote Sensing*, 7, 600-626; doi:10.3390/rs70100600.

2014 Markham, B., Barsi, J., Kvaran, G., Ong, L., Kaita, E., Biggar, S., Czapla-Myers, J., Mishra, N., Helder, D. (2014) Landsat-8 Operational Land Imager Radiometric Calibration and Stability. *Remote Sensing*, 6, 12275-12308; doi:10.3390/rs61212275.

Technical Description of Images:

Figure 1. A Landsat-8 TIRS image of the coast of Southern California showing the effect of stray light on the imagery before and after the operational stray light correction to go into effect in November 2016.

Figure 2. The Landsat-8 OLI radiometric response trends to the on-board calibration systems and the moon demonstrating the stability of band 2 of the OLI instrument to the ±0.2% level. Other bands are similar, with only band 1 showing a 1% change over three years; the November 2016 processing update will adjust for this change.

Figure 3. A comparison of the OLI radiometric calibration to the similar bands of the Sentinel-2 MSI instrument. With the exception of band 1 at ~5% difference, the bands are within ~1%.

Scientific significance:

Accuracy within and consistency between data products Is critical for any scientific analysis combining data sources and/or evaluating Earth surface changes. Long term consistency of the Landsat data record has been achieved and consistency between Landsat and Sentinel-2 data will allow combining data from these two platforms to achieve Earth coverage at the 2-3 day interval.

Relevance for future science and relationship to Decadal Survey:

The TIRS stray light has limited the ability to determine absolute temperature of targets– the correction algorithm should reduce TOA uncertainty to ~1K for most scenes. With the consistency within the Landsat data record scientists will be able to assess Earth surface trends across ~35 years (with TM quality or better data) and ~45 years (when MSS data are included). With multiple Landsat and Sentinel-2 sensors operating simultaneously, the data consistency will allow within season phenological studies at moderate (30 meter or better) spatial resolution, not heretofore possible.

Oldest sea ice disappearing in the Arctic Ocean

Walt Meier[1], Mark Tschudi[2] and Scott Stewart[2]

[1]Cryospheric Sciences Lab, NASA GSFC , [2]National Snow and Ice Data Center

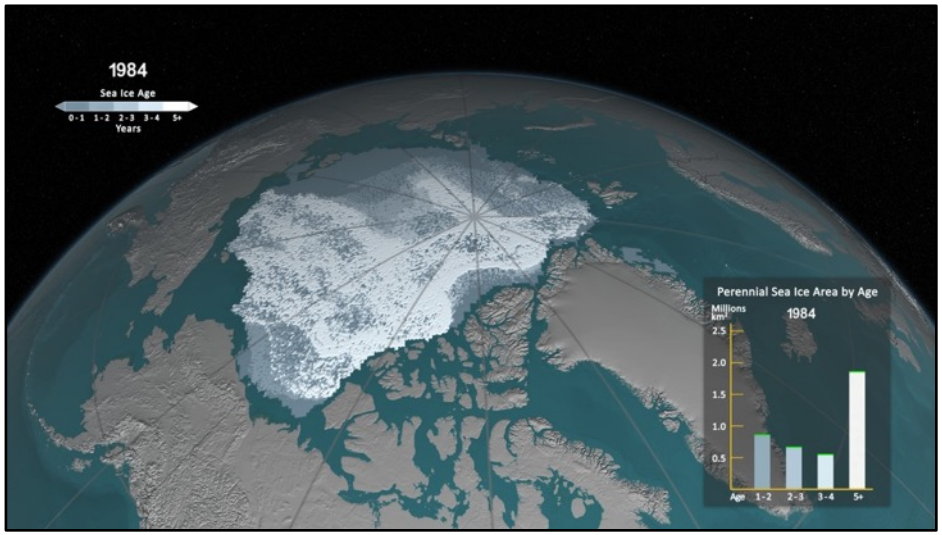

Figure 1

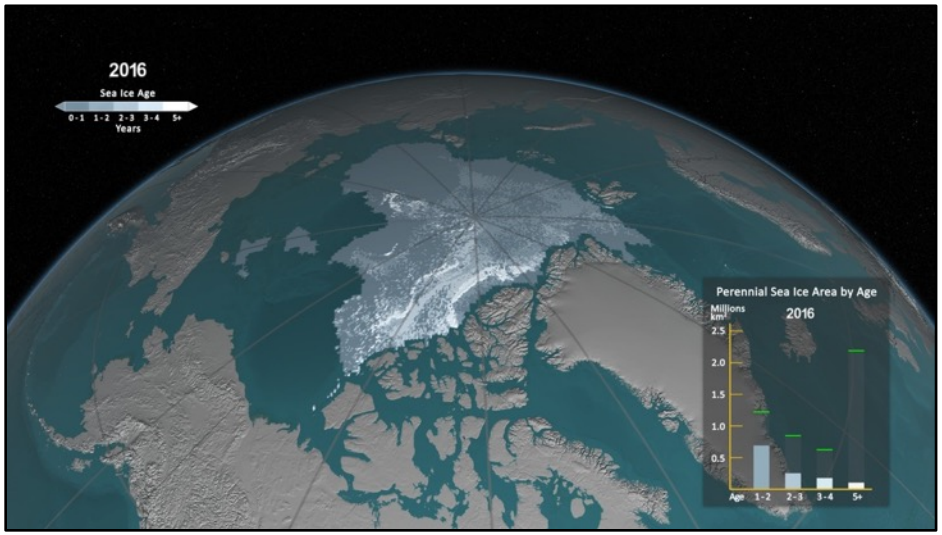

Figure 2

September minimum extent was 4.14 x 10^6 km^2, tied with 2007 for 2nd lowest in the satellite era (since 1979) and the ice cover is much younger and thus on average much thinner than it once was. Perennial ice (ice that survived at least one summer) once covered most of the Arctic Ocean. Perennial has declined precipitously and now the oldest ice (5+ year old) has almost completely disappeared from the Arctic.

Name: Walt Meier, Cryospheric Science Lab, NASA GSFC
E-mail: walt.meier@nasa.gov
Phone: 301-614-6572

References:

Tschudi, M., C. Fowler, J. Maslanik, J. S. Stewart, and W. Meier, 2016. EASE-Grid Sea Ice Age, Version 3. Boulder, Colorado USA. NASA National Snow and Ice Data Center Distributed Active Archive Center. doi: 10.5067/PFSVFZA9Y85G.

Tschudi, M.A., Stroeve, J.C., and Stewart, J.S., 2016. Relating the Age of Arctic Sea Ice to its Thickness, as Measured during NASA's ICESat and IceBridge Campaigns. *Remote Sensing*, 2016, 8, 457, doi:10.3390/rs8060457.

Meier, W.N., J.A. Maslanik, and C.W. Fowler, 2000. Error analysis and assimilation of remotely sensed ice motion within an Arctic sea ice model*, Journal of Geophysical Research*, 105(C2), 3339–3356, doi:10.1029/1999JC900268.

Data Sources: Passive microwave imagery from NASA AMSR-E and DMSP SSMI and SSMIS, AVHRR, NCEP Reanalyses, and International Arctic Buoy Programme buoys are used for the product. The images were created by the NASA Scientific Visualization Studio at Goddard (special thanks to Cindy Starr, SVS).

Technical Description of Figures: The images show sea ice age at the end of the summer melt season in September. The whitest regions are the oldest ice. The darkest gray color is ice that is less than one year old.

Figure 1: September 1984, showing old ice covering most of the Arctic Ocean.

Figure 2: September 2016, with very little white.

In Figures 1 and 2, the inset bar graphs in the lower right indicate the area of each ice age category more than one year old; the green bars in both insets are the values for 1984. The sea ice age is derived from satellite imagery via Lagrangian tracking of ice using cross-correlation feature matching between pairs of co-located images separated by time. Motions are derived from wind-forcing via an empirically-derived rule-of-thumb scaling (ice moves 1-2% of the wind speed, ~30 degrees to the right). The different sources are combined via an optimal interpolation scheme that takes account of the spatial distribution and the relative error characteristics of each observation.

Scientific significance, societal relevance, and relationships to future missions: While the downward trend in sea ice extent is well known from remote sensing, changes in thickness are much less complete. Satellite altimetry has started to provide Arctic-wide data since the NASA ICESat mission began in 2003 and observations have continued with Operation IceBridge. But neither can provide full temporal and spatial coverage or a long historical record. The ice age product provides a longer term context for ICESat and IceBridge, as well as the upcoming ICESat-2 mission. We are also investigating the potential to use the Lagrangian tracking for other important Arctic parameters such as: cumulative fluxes, melt, and snow accumulation. This will allow us to better observe the evolution of the Arctic system as well as provided improved inputs into other satellite products such as ICESat-2.

Evaluating multi-spectral snowpack reflectivity with changing snow grain sizes

DK Kang[1,3], Ana Barros[2], and Edward Kim[3], Hydrological Sciences,
[1]UMD ESSIC, [2]Duke Uni., [3]NASA GSFC

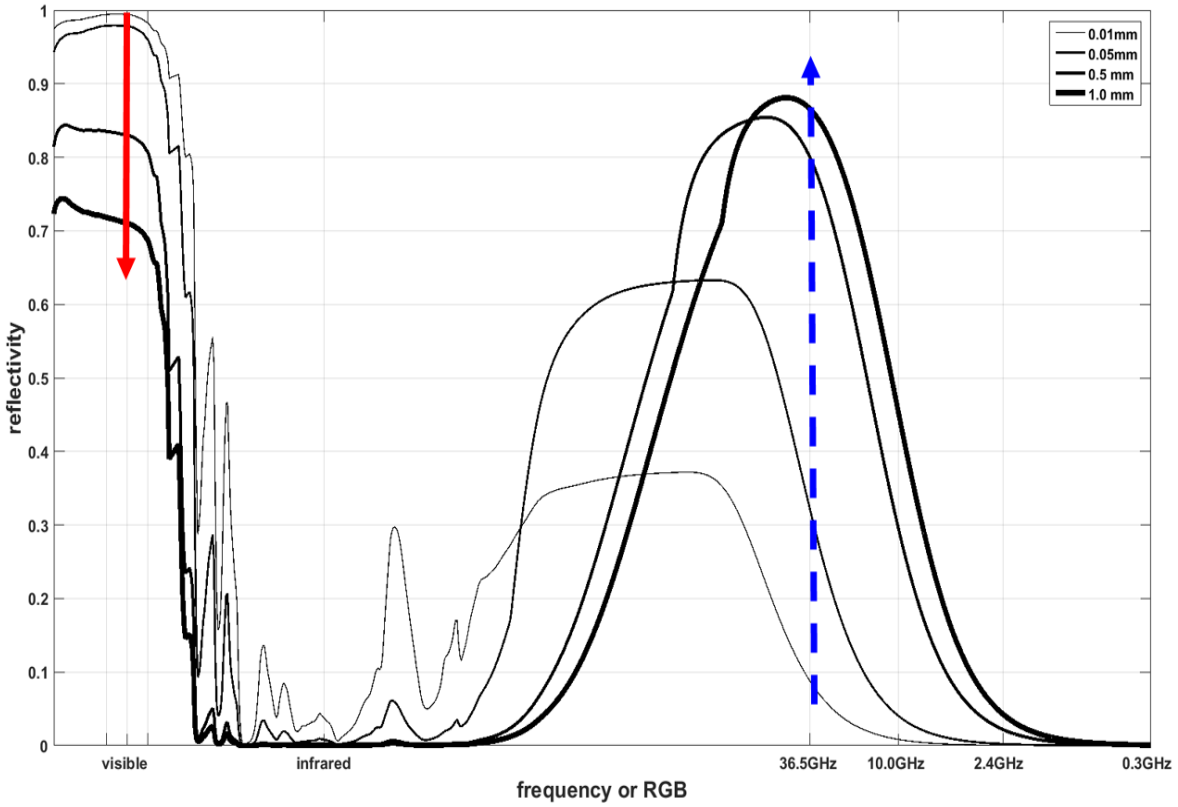

Figure 1

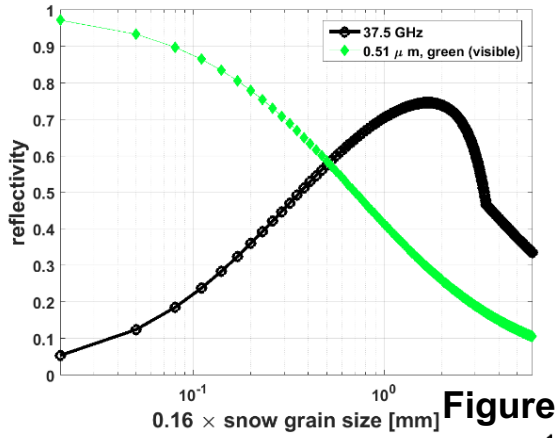

Figure 2

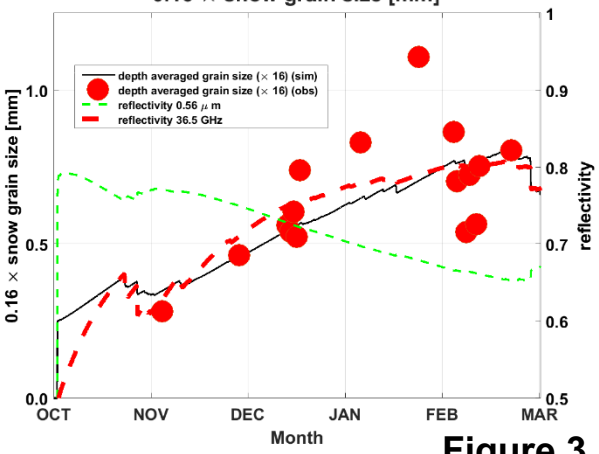

Figure 3

A radiative transfer model that simulates snow surface reflectivity from visible to microwave frequencies suggests the potential to develop a unified retrieval algorithm for snow microphysical properties from remote sensing. This unified approach is directly used to extract snow microphysical properties (grain size, texture, roughness, etc.) from aircraft and satellite remote sensing regardless of the observed wavelength.

Name: Edward Kim, Hydrological Sciences, NASA GSFC
E-mail: ed.kim@nasa.gov
Phone: 301-614-6569

References:

2000 Mätzler, C., "*A simple snowpack/cloud reflectance and transmittance model from microwave to ultraviolet: the ice-lamella pack*," *Journal of Glaciology*, vol. 46, pp. 20-24, 2000.

2012 Kang, D., and Barros, A. P., "*Observing system simulation of snow microwave emission s over data sparse regions. Part2: Multi-layer physics*," *IEEE Transactions on Geoscience and Remote Sensing*, vol. 50, pp. 1806-1820.

2005 Graf, T., Koike, T., Fujii, H., et al.. "*Observations of Snow Properties, Meteorological Forcing and Brightness Temperature Data at the Local Scale Observation Site during the Cold Land Processes Field Experiment and the Application to a Dense Media Radiative Transfer Model*." *Ann J Hydraulic Eng*, **49:** 7.

Technical Description of Images:

Figure 1. Snow reflectivity sensitivity to snow grain size (×0.16) (0.01, 0.05, 0.5, and 1.0 mm) from the UV to microwave frequencies. solid and dashed arrows indicate a reflectivity decrease in the visible range and an increase in the microwave range, respectively. The simulated snow was dry, containing 0.2 meter snow water equivalent, 1 meter snow depth and snow density of 200 kg m^{-3}.

Figure 2. Reflectivity variation with snow grain size in the visible (0.51μm, 535.34 THz), and microwave (8 mm, 36.5 GHz) wavelengths. The dry snow contains 0.2 meter snow water equivalent, 1 meter snow depth and snow density of 200 kg m^{-3}.

Figure 3. Temporal evolution of snow surface reflectivity compared both with simulated and observed snow grain size (×0.16) in the visible (0.56μm), and microwave (36.5 GHz, 8.2 mm) wavelengths.

Scientific significance:

Terrestrial snow retrieval algorithms with remote sensing have been developed depending on electromagnetic channels mainly divided with visible and microwave frequencies. This research can initiate a potential approach to implement a unified version of retrieval algorithm for the snow microphysics properties leading to snow surface reflectivity regardless of wavelengths.

Relevance for future science and relationship to Decadal Survey:

A terrestrial snow plays an essential role in water resources management in dry western US and Canada and mountainous regions in the world. With a climate change, it also poses one of the most sensitive variables dependent upon air temperature changes. However, owing to the physical dimensions of the sensor specifications, optical and microwave sensors have been developed separately and the retrieval algorithms for the terrestrial snow have been disjointly developed. This research thus can provide one of solutions to an upcoming unified retrieval model to estimate snow surface microphysics which are important to simulate radar responses and optical detections observed in remote sensors in aircrafts and satellites for the future land-snow missions.

A method for improving MODIS hotspot directional signatures

[1]Miguel O. Román and [1]Zhuosen Wang, [2]Charles Gatebe and [2]Rajesh Poudyal,
[1]Terrestrial Information Systems, NASA GSFC, [2]Climate and Radiation Laboratory, NASA/GSFC

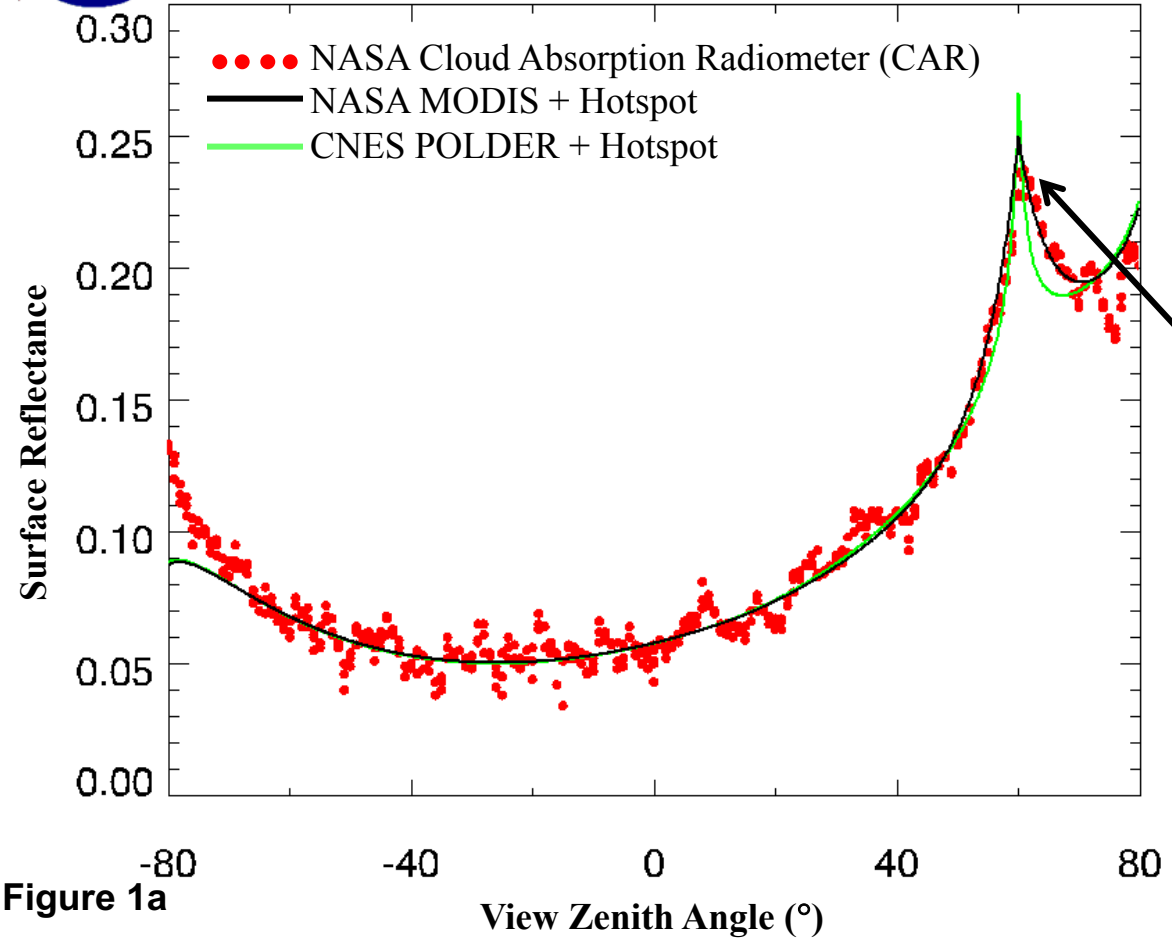

Figure 1a

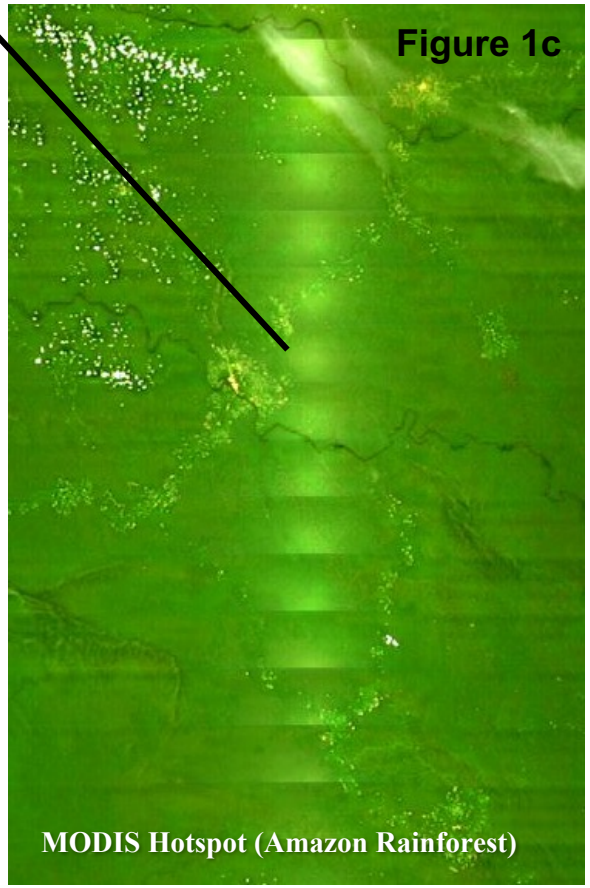

NASA airborne measurements were used to improve MODIS BRDF retrievals over the Amazon forest. Incorporating these improvements in MODIS Land products will enable scientists to characterize vegetation structure and function on a global scale.

Name: Miguel O. Román, Terrestrial Information Systems, NASA GSFC
E-mail: miguel.o.roman@nasa.gov
Phone: 301-614-5498

References:

Jiao, Z., Schaaf, C.B., Dong, Y., Román, M.O., Hill, M.J., Chen, J.M., Wang, Z., Zhang, H., Saenz, E., Paudyal, R., Gatebe, C., Breon, F., Li, X., Strahler, A. (2016), A method for Improving hotspot directional signatures in BRDF models used for MODIS. *Remote Sensing of Environment*, 186,135–151

Román, M.O., Gatebe, C.K., Schaaf, C.B., Poudyal, R.,Wang, Z., King, M.D. (2011). Variability in surface BRDF at different spatial scales (30 m–500 m) over a mixed agricultural landscape as retrieved from airborne and satellite spectral measurements. *Remote Sensing of Environment*. 115, 2184–2203

Chen, J.M., Cihlar, J. (1997). A hotspot function in a simple bidirectional reflectance model for satellite applications. *Journal of Geophysical Research: Atmospheres*. 102, 25907–25913.

Data Sources:

Measurements acquired from POLDER-3 sensor onboard the Polarization and Anisotropy of Reflectances for Atmospheric Sciences coupled with Observations from a Lidar (PARASOL) satellite were used to improve models of the Bidirectional Reflectance Distribution Function (BRDF). MODIS surface reflectance products (MOD/MYD09) and BRDF/albedo products(MCD43) were downloaded from NASA LAADS website. High spatial resolution airborne multi-angular airborne measurements collected by NASA's Cloud Absorption Radiometer (CAR) were used as reference data.

Technical Description of Figures:

Figure 1a: Comparison of NASA airborne Cloud Absorption Radiometer (CAR) angular measurements with BRDF model fitted MODIS and POLDER reflectances along principle plane. Hotspot function is integrated into the BRDF model.

Figure 1b: NASA P3B aircraft with CAR instrument in nose cone .

Figure 1c: MODIS reflectance at Amazon forest. The bright region is around the hotspot area where sun is behind sensor and shadows are hidden.

Scientific significance, societal relevance, and relationships to future missions: A new method is developed to improve the hotspot effects of MODIS directional signatures. With the hotspot-related model parameters determined, this method offers improved performance for various ecological remote sensing applications including the estimation of canopy structure parameters. The diversity of Earth's vegetation requires that a variety of remote sensing approaches be combined in order to attempt to capture the three dimensional variation that significantly influences terrestrial ecosystems. A large number of factors have been shown to be highly influential on vegetation trends and dynamics including canopy height, tree density, leaf area index (LAI) and canopy cover. If some of these factors can be defined with multiple satellite sensors, then scientists can calibrate these measurements to specific ecosystems. In this respect, sustained observations (e.g., MODIS, VIIRS, Landsat) can be used in conjunction with full waveform LiDAR (such as GEDI) to get a complete mapping of the canopy structure over a forested scene.